



1 **First Measurement of Atmospheric Mercury Species in Qomolangma Nature**

2 **Preserve, Tibetan Plateau, and Evidence of Transboundary Pollutant Invasion**

3 **Authors**

4 Huiming Lin¹, Yindong Tong^{2*}, Xiufeng Yin^{3,4,5}, Qianggong Zhang^{4,6}, Hui Zhang⁷, Haoran Zhang¹,

5 Long Chen⁸, Shichang Kang^{3,5,6}, Wei Zhang⁹, James Schauer^{10,11}, Benjamin de Foy¹², Xiaoge Bu²,

6 Xuejun Wang^{1**}

7 **Affiliations**

8 1. MOE Laboratory of Earth Surface Processes, College of Urban and Environmental Sciences,

9 Peking University, Beijing, 100871, China;

10 2. School of Environmental Science and Engineering, Tianjin University, Tianjin, 300072, China;

11 3. State Key Laboratory of Cryospheric Science, Northwest Institute of Eco-Environment and

12 Resources, Chinese Academy of Sciences, Lanzhou, 730000, China;

13 4. Key Laboratory of Tibetan Environment Changes and Land Surface Processes, Institute of

14 Tibetan Plateau Research, Chinese Academy of Sciences, Beijing, 100101, China;

15 5. University of Chinese Academy of Sciences, Beijing, 100039, China;

16 6. CAS Center for Excellence in Tibetan Plateau Earth Sciences, Beijing, 100085, China;

17 7. State Key Laboratory of Environmental Geochemistry, Institute of Geochemistry, Chinese

18 Academy of Sciences, Guiyang, 550002, China;

19 8. School of Geographic Sciences, East China Normal University, Shanghai, 200241, China;

20 9. School of Environment and Natural Resources, Renmin University of China, Beijing, 100872,

21 China;

22 10. Department of Civil and Environmental Engineering, University of Wisconsin-Madison, WI,

23 53706, USA;

24 11. Wisconsin State Laboratory of Hygiene, University of Wisconsin-Madison, WI, 53706, USA;

25 12. Department of Earth and Atmospheric Sciences, Saint Louis University, MO, 63108, USA;

26 **Correspondence:**

27 *Yindong Tong, Tianjin University, Tianjin, China, Email at: yindongtong@tju.edu.cn;

28 **Xuejun Wang, Peking University, Beijing, China, Email at: wangxuejun@pku.edu.cn;

29



30 Abstract

31 Located in the world's 'Third Pole' and a remote region connecting the Indian
32 Ocean plate and the Eurasian plate, Qomolangma National Nature Preserve (QNNP)
33 is an ideal region to study the long-range transport of atmospheric pollutants. In this
34 study, gaseous elemental mercury (GEM), gaseous oxidized mercury (GOM) and
35 particle-bound mercury (PBM) were continuously measured during the Indian
36 monsoon transition period in QNNP. A slight increase in GEM concentration was
37 observed from the period preceding the Indian Summer Monsoon ($1.31 \pm 0.42 \text{ ng m}^{-3}$)
38 to the Indian Summer Monsoon period ($1.44 \pm 0.36 \text{ ng m}^{-3}$), while significant decreases
39 were observed in GOM and PBM concentrations, decreasing from 35.2 ± 18.7 to
40 $19.1 \pm 11.0 \text{ pg m}^{-3}$ and from 30.5 ± 12.6 to $24.7 \pm 19.9 \text{ pg m}^{-3}$, respectively. A unique
41 daily pattern of GEM concentration in QNNP was observed, with a peak value before
42 sunrise and a low value at noon. Unexpectedly, GOM concentrations (with a mean
43 value of $21.3 \pm 13.5 \text{ pg m}^{-3}$) in this region were considerably higher than the values in
44 other clean or even polluted regions. A cluster analysis indicated that the air masses
45 transported to QNNP changed significantly at different stages of the monsoon, and the
46 major potential Hg sources shifted from north India and west Nepal to east Nepal and
47 Bangladesh. With large coverage of glacier in QNNP, local glacier winds could
48 enforce the transboundary transport of pollutants and transport the polluted air masses
49 to the Tibetan Plateau. It should be noted that the atmospheric Hg concentrations in
50 QNNP are higher than the reported values in some background regions, which
51 addresses the need for a more specific identification of Hg sources in QNNP and the
52 importance of international cooperation for global Hg controls.

53 Keywords

54 Indian summer monsoon; atmospheric mercury; trans-boundary transport; glacier
55 winds; Qomolangma National Nature Preserve

56 1. Introduction

57 Understanding of atmospheric mercury (Hg) concentration in remote regions is
58 vital to understand the global atmospheric Hg cycling processes (UNEP, 2013; Angot



59 et al., 2016; Zhang et al., 2016a). Generally, atmospheric Hg can be divided into three
60 major types: gaseous elemental Hg (GEM), gaseous oxidized Hg (GOM) and
61 particle-bound Hg (PBM) (Fu et al., 2010). Over 95% of atmospheric Hg exists in the
62 form of GEM (Ebinghaus et al., 2002; Huang et al., 2014). Due to its stable chemical
63 properties and long half-life in the atmosphere (approximately 1-2 years), GEM can
64 be transported over long distances easily (Fang et al., 2009). In contrast, GOM and
65 PBM can be deposited quickly from the atmosphere, exposing local environments to
66 significant impacts (Lindberg and Stratton, 1998; Seigneur et al., 2006; Lynam et al.,
67 2014). To understand the global and regional cycling of atmospheric Hg, different Hg
68 monitoring networks and sites have been established in recent decades, such as the
69 Atmospheric Mercury Network (AMNet) (Gay et al., 2013) and Global Mercury
70 Observation System (GMOS), which contains over 40 ground-based monitoring
71 stations distributed in the world (Sprovieri et al., 2016). Generally, atmospheric Hg
72 background concentrations range between 1.5-1.7 and 1.1-1.3 ng m⁻³ in the northern
73 and southern hemisphere, respectively (Lindberg et al., 2007; Slemr et al., 2015;
74 Venter et al., 2015). However, the existing studies are still far from sufficient to obtain
75 a full understanding of long-range Hg transport due to inadequate monitoring data in
76 the remote and less-populated regions (Fu et al., 2012a; Zhang et al., 2015a).

77 The trans-boundary and long-range transport of pollutants have attracted
78 considerable attention (Zhang et al., 2015b; Li et al., 2016; Pokhrel et al., 2016; Yang
79 et al., 2018) in the northeastern and southeastern regions of the Tibetan Plateau. The
80 transboundary invasions of atmospheric pollutants in the Tibetan Plateau have been
81 evidenced in pollutants such as persistent organic pollutants and black carbon (Zhang
82 et al., 2015b; Li et al., 2016; Pokhrel et al., 2016; Yang et al., 2018). It was reported
83 that smoke from biomass burning in the Indian subcontinent could pass through the
84 natural barrier of the Himalaya (Wang et al., 2015; Pokhrel et al., 2016). HCHs, DDTs
85 and PCBs were all found to have their highest concentrations in the southeast Tibetan
86 Plateau during the monsoon season (Wang et al., 2018). Similar conditions have also
87 occurred for black carbon (Li et al., 2016). However, studies of the trans-boundary



88 transport of Hg on the Tibetan Plateau are still limited. The existing Hg monitoring
89 data is affected to varying extents by local emission sources (Fu et al., 2012a; Zhang
90 et al., 2015; Zhang et al., 2016). The atmospheric Hg concentrations in Waliguan,
91 located at the northeastern edge of the Tibetan Plateau, originated from or passed
92 through the urban and industrial areas in Western China and Northern India (Fu et al.,
93 2012a). Located at the southeastern edge of the Tibetan Plateau, the atmospheric Hg
94 sources for Shangri-La are Southeast Asia, India and mainland China (Zhang et al.,
95 2015a). Furthermore, studies are still lacking on trans-boundary transport of Hg in the
96 Qomolangma National Nature Preserve (QNNP), which directly connects the Indian
97 Subcontinent and Eurasia. The detailed pollutant transport pathways and seasonal or
98 daily patterns of atmospheric Hg concentrations in this region are still not clear.

99 QNNP, located at the southern edge of the Tibetan Plateau, is considered one of the
100 world's cleanest regions (Qiu, 2008). With an average altitude of ~4,500 m a.s.l.,
101 QNNP is a remote region with sparse human population and rare industries (Qiu,
102 2008; Yao et al., 2012b; Li et al., 2016). However, it is surrounded by two large
103 potential pollution sources: the populated and developed eastern China region, which
104 has experienced about 30 years of quick industrial development, and South Asian
105 developing countries (e.g., India, Nepal, and Bangladesh), which have been
106 developing at a quick rate in recent years (Streets et al., 2011; Zhang et al., 2015b;
107 Yang et al., 2018). China and India are reported as the largest coal consumers in the
108 world (BP Statistical Review of World Energy 2018), and coal combustion is the
109 largest source of atmospheric Hg emissions, supplying ~86% of Hg emissions from
110 fuel combustion (Chen et al., 2016). With QNNP located at the air mass transport
111 pathway of the Indian Summer Monsoon (ISM) (Li et al., 2016), meteorological
112 conditions in QNNP vary significantly during the monsoon transition period (Wang et
113 al., 2001). The monthly average precipitation can range from <50 mm in the non-ISM
114 period to 950 mm in the ISM period (Panthi et al., 2015). In addition to the monsoon,
115 with a glacial coverage of ~2,710 km² in QNNP (Nie et al., 2010), glacier winds could
116 also have direct effects on the local pollutant transport because glacier winds can



117 pump down polluted air from the upper levels of the stratosphere to the land surface
118 (Cai et al., 2007). Therefore, the atmosphere in QNNP is vulnerable to the
119 surrounding pollution sources (Xu et al., 2009; Li et al., 2016).

120 To the best of our knowledge, the present work is the first study regarding Hg
121 monitoring and source identification covering both the preceding-Indian Summer
122 Monsoon (PISM) and ISM periods in the QNNP. This monitoring site is unique
123 because it is located in the air mass transport pathway from South Asia to the Tibetan
124 Plateau. We performed comprehensive and continuous measurements of GEM, GOM
125 and PBM concentrations during the onset and process period of the Indian monsoon.
126 To identify the detailed sources, we also combined the real-time Hg monitoring data
127 with a backward trajectory analysis, clustering analysis and potential source
128 contribution function (PSCF) analysis. The effects of local glacier winds, caused by
129 large coverages of QNNP glaciers, on the trans-boundary transport of pollutants were
130 discussed. This combined monitoring and modeling study could help researchers and
131 government managers to accurately understand the global Hg cycling process and
132 potential impacts from the rapidly developing countries in South Asia on the
133 atmospheric Hg concentrations in QNNP.

134 **2. Materials and methods**

135 **2.1 Atmospheric Hg monitoring site**

136 Atmospheric Hg monitoring was conducted at “Atmospheric and Environmental
137 Comprehensive Observation and Research Station, Chinese Academy of Sciences on
138 Mt. Qomolangma” (latitude: 28°21’54” N, longitude: 86°56’53” E) in QNNP, at an
139 altitude of 4,276 m a.s.l. (Figure 1). In QNNP, Mt. Qomolangma spreads from east to
140 the west along the border between the Indian subcontinent and the Tibetan Plateau
141 (Figure 1). Due to the high altitude, QNNP is naturally isolated from the populated
142 regions, and rare local Hg emission sources have been observed (UNEP, 2013). The
143 most populated region near this monitoring site is Tingri County (with a population
144 density of 4 persons per km²), located ~40 km to the southwest of the monitoring site.
145 QNNP is located in the air mass transport pathway of the ISM (Li et al., 2016), and



146 the meteorological conditions in QNNP have significant variations between the PISM
147 and ISM periods (Wang et al., 2001). During the transition period, the temperature in
148 the Tibetan Plateau and South Asia changes from “southern warm - northern cool” to
149 “northern warm - southern cool” (Wang et al., 2001). This reverse leads to a
150 significant increase of diabatic heating over South Asia and the southern slope of the
151 Tibetan Plateau (Ge et al., 2017), which further affects the wind directions and speeds.
152 Local glacier winds could also affect the transport of air masses in QNNP. Glaciers
153 cover $\sim 2,710 \text{ km}^2$ in QNNP (Nie et al., 2010), and most of the glaciers are located on
154 the northern slope of the mountain (Figure 1) (Bolch et al., 2012). The glacier wind is
155 a continuous downslope wind blowing from glacier surfaces down to the foothills of
156 the mountain throughout the day. Hence, the transport of air masses in this region is a
157 combination of atmospheric circulation (monsoon) and local weather conditions
158 (glacier winds). The structure of the boundary layer over QNNP is also significantly
159 affected by glaciers (Li et al., 2006). The height of the atmospheric boundary layer
160 changes significantly in one day from $\sim 350 \text{ m}$ above the ground level during the night
161 to $\sim 2000 \text{ m}$ during the day.

162 **2.2 GEM, GOM and PBM monitoring**

163 To describe the changes of atmospheric Hg concentrations during the PISM and
164 ISM periods, the real-time continuous measurements of GEM, GOM and PBM
165 concentrations were carried out using the Tekran 2537B, 1130 and 1135 instruments
166 (Tekran Inc., Toronto, Canada) from 15 April, 2016 to 14 August, 2016. During the
167 operation of the Tekran instruments, ambient air was introduced into the instrument
168 for 60 minutes through an impactor, a KCL-coated annular denuder, and a Quartz
169 Fiber Filter (QFF). All the Hg species were converted into Hg(0) and then measured
170 by cold vapor atomic fluorescence spectroscopy (CVAFS). The collected PBM and
171 GOM were desorbed in succession to Hg(0) at the temperature of $800 \text{ }^\circ\text{C}$ and $500 \text{ }^\circ\text{C}$,
172 respectively. Hg-free air was used to flush the 1130 and 1135 systems to introduce the
173 desorbed PBM and GOM into model 2537B for analysis. The sampling inlet was set
174 at $\sim 1.5 \text{ m}$ above the instrument platform (shown in Figure S1). To mitigate the



175 impacts of low atmospheric pressures on the pump's train, a low air sampling rate of 7
176 L min⁻¹ for the pump model and 0.75 L min⁻¹ (at standard pressure and temperature)
177 for model 2537B was applied (Swartzendruber et al., 2009; Zhang et al., 2015a;
178 Zhang et al., 2016a). The Tekran 2537B analyzer was calibrated automatically using
179 the internal Hg permeation source inside the instrument every 23 h, and the internal
180 source was calibrated before and after the monitoring by an external Hg source using
181 a syringe. The Tekran ambient Hg analyzer has been described in more details in the
182 previous publications (Landis et al., 2002; Rutter et al., 2008; de Foy et al., 2016).

183 **2.3 Meteorological data**

184 Throughout the sampling period, the meteorological information was recorded
185 using the Vantage Pro2 weather station (Davis Instruments, USA) with a 5-minute
186 resolution. The monitored parameters included the temperature (with a precision of
187 0.1 °C), relative humidity (with a precision of 1%), wind speed (with a precision of 0.1
188 m s⁻¹), wind direction (with a precision of 1 °), air pressure (with a precision of 0.1
189 hPa), solar radiation (with a precision of 1 W m⁻²) and UV index (with a precision of
190 0.1 MEDs). The snow cover data was obtained from the Moderate Resolution
191 Imaging Spectroradiometer (MODIS) instrument on board the Terra and Aqua
192 satellites (MOD10A1, Hall et al., 2010) with a daily 0.05 ° resolution.

193 **2.4 Backward trajectory simulation**

194 To identify the atmospheric Hg sources, the Hybrid Single-Particle Lagrangian
195 Integrated Trajectory (HYSPLIT) model was applied to perform a backward trajectory
196 simulation (Stein et al., 2015; Chai et al., 2016; Chai et al., 2017; Hurst and Davis,
197 2017). The HYSPLIT model, known as a complete and mature system for modeling
198 simple air parcel trajectories of complex pollutant dispersion and deposition, was
199 developed by the US National Oceanic and Atmospheric Administration (NOAA).
200 Global Data Assimilation System (GDAS) data with 1 °×1 ° latitude and longitude
201 horizontal spatial resolution and 23 vertical levels at 6-hour intervals was used for the
202 backward trajectory simulation. All the trajectory arrival heights were set at 1500 m
203 above ground level. Every backward trajectory was set for 72 hours in 6-hour



204 intervals, and the air mass transport regions covered China, Nepal, India, Pakistan and
205 majority of west Asia. Backward trajectories during the whole monitoring period were
206 calculated, and cluster analysis was carried out to identify the Hg transport pathways.
207 The cluster statistics summarize the percentage of back trajectories in each cluster,
208 and the average GEM concentrations are linked with each cluster. The clustering
209 algorithm utilized in this study is based on Ward's hierarchical method (Ward Jr,
210 1963), and minimizing angular distances between corresponding coordinates of the
211 individual trajectories were chosen to calculate the clusters. By averaging similar or
212 identical pathways from existing air mass pathways to the receiving site, clusters can
213 help identify the mean transport pathways of air masses and provide the primary
214 directions of pollutants transported to the receiving site.

215 The Potential Source Contribution Function (PSCF) model is a hybrid receptor
216 model using the calculated backward trajectories to estimate the contributions of
217 different emission sources in upwind regions and has been applied in many previous
218 studies (Kim et al., 2005; Kaiser et al., 2007; Fu et al., 2012b; Zhang et al., 2013). The
219 PSCF calculation is made based on counting the trajectory segments that terminate
220 within each cell to determine the values for the grid cells in the study domain
221 (Ashbaugh et al., 1985). In this study, the PSCF model was used to identify the
222 possible sources of atmospheric GEM. The study domain was separated as $i \times j$ cells.
223 Then, the PSCF value for the ij^{th} cell is defined as follows:

$$224 \quad PSCF_{ij} = \frac{M_{ij}}{N_{ij}}$$

225 where N_{ij} is the total number of endpoints that fall into ij^{th} cell during the whole
226 simulation period, and M_{ij} is the number of endpoints for the same cell that
227 correspond to GEM concentrations higher than a set criterion. In this study, PSCF
228 values were calculated based on the average GEM concentration during the whole
229 sampling campaign. The PSCF value stands for the conditional probability that the
230 GEM concentration at the measurement site is larger than the average GEM
231 concentration if the parcel passes through the ij^{th} cell before it reaches the
232 measurement site.



233 To account for and reduce the uncertainty due to low values of N_{ij} , the PSCF values
234 were scaled by an arbitrary weighting function W_{ij} (Polissar et al., 1999). While the
235 total number of the endpoints in a cell (N_{ij}) is less than ~three times the average value
236 of the end points for each cell, the weighting function will decrease the PSCF values.
237 In this study, W_{ij} was set using the following piecewise function:

$$W_{ij} = \begin{cases} 1.00 & N_{ij} > 3 N_{ave} \\ 0.70 & 3 N_{ave} > N_{ij} > 1.5 N_{ave} \\ 0.42 & 1.5 N_{ave} > N_{ij} > N_{ave} \\ 0.05 & N_{ave} > N_{ij} \end{cases}$$

238 Combining the MODIS fire spots data, we used the PSCF analysis to validate the
239 effects of biomass burning regions. MODIS fire spots data (from 1 April 2016 to 31
240 August 2016) was obtained from the Fire Information for Resource Management
241 System (FIRMS) operated by the National Aeronautics and Space Administration
242 (NASA) of the United States (Giglio et al., 2003; Davies et al., 2004).

243 3. Results and discussion

244 3.1 Comparisons of atmospheric Hg concentrations between PISM and ISM

245 The GEM, GOM and PBM concentrations at the sampling site were 1.42 ± 0.37 ng
246 m^{-3} , 21.3 ± 13.5 pg m^{-3} and 25.5 ± 19.2 pg m^{-3} , respectively, during the whole study
247 period (Figure 2 and Table 1). GEM accounted for over 95% of all the Hg species.
248 Figure S2 shows a comparison of the GEM, GOM and PBM concentrations during the
249 PISM and ISM periods. During the PISM period, the average GEM, GOM and PBM
250 concentrations were 1.31 ± 0.42 ng m^{-3} , 35.2 ± 18.7 pg m^{-3} , and 30.5 ± 12.6 pg m^{-3} ,
251 respectively, while during the ISM period, the average GEM, GOM and PBM
252 concentrations were 1.44 ± 0.36 ng m^{-3} , 19.1 ± 11.0 pg m^{-3} , and 24.7 ± 19.9 pg m^{-3} ,
253 respectively. We further compared the Hg concentrations at different ISM stages.
254 Figure S2 shows that GEM concentrations increased significantly with the
255 development of the ISM, while decreases of GOM and PBM concentrations were
256 observed during the study period, with a decrease of 39.0% (the average concentration
257 change from 20.20 pg m^{-3} to 12.33 pg m^{-3}) and 49.6% (the average concentration
258 change from 21.18 pg m^{-3} to 10.68 pg m^{-3}), respectively.



259 Table 2 summarizes GEM, GOM and PBM concentrations and diurnal variations of
260 GEM measured by the Tekran system globally. Generally, the GEM concentration in
261 the QNNP was approaching the reported values in the Northern Hemisphere (~ 1.5 - 1.7
262 ng m^{-3}) and was higher than those in the Southern Hemisphere (~ 1.1 - 1.3 ng m^{-3})
263 (Lindberg et al., 2007; Slemr et al., 2015; Venter et al., 2015). Among the global Hg
264 monitoring sites, the EvK2CNR monitoring site on the southern slope of the Tibetan
265 Plateau, Nepal, is the nearest station (at a straight-line distance of approximately 50
266 km) from the monitoring site in this study (Gratz et al., 2013). The average GEM
267 concentration at EvK2CNR (1.2 ± 0.2 ng m^{-3} , from Nov. 2011-Apr. 2012) was slightly
268 lower than that in the QNNP (1.31 ± 0.42 ng m^{-3} during the PISM period and
269 1.44 ± 0.36 ng m^{-3} during the ISM period). Compared to Hg concentrations observed at
270 China's background stations and rural regions (e.g., Waliguan Baseline Observatory
271 (1.98 ± 0.98 ng m^{-3}) (Fu et al., 2012a), Ailaoshan Mountain National Natural Reserve
272 (2.09 ± 0.63 ng m^{-3}) (Zhang et al., 2016a), and Shangri-La Baseline Observatory in
273 Yunnan province (2.55 ± 0.73 ng m^{-3}) (Zhang et al., 2015a)), the average GEM
274 concentration in the QNNP was lower. However, it should be noted that GOM
275 concentrations (with a value of 21.3 ± 13.5 pg m^{-3}) in this region were much higher
276 than the values in clean regions (usually lower than 10 pg m^{-3}) and a known polluted
277 region (the suburban area of Beijing (10.1 ± 18.8 pg m^{-3}) (Zhang et al., 2013) (Table 2).
278 One possible explanation for the high GOM concentration is the strong subsidence in
279 QNNP. The subsidence of the free troposphere would bring GOM-enriched air masses
280 to the surface layer (Fa ñ et al., 2009), resulting in the observed high surface GOM
281 levels (Weiss - Penzias et al., 2009). In QNNP, with the wide distribution of glaciers,
282 glacier winds could bring the upper air masses to the land surface layer (Song et al.,
283 2007), which could further strengthen the subsidence movement.

284 The increases of GEM concentrations during the ISM period could indicate the
285 impacts of trans-boundary transport, which has been confirmed by the previous
286 studies (Fu et al., 2012a; Zhang et al., 2016a). The deposition of GEM from the
287 atmosphere to the land surface is difficult, and GEM has a much longer residence



288 time than the other Hg species (Fang et al., 2009), making it a good tracer that can
289 represent the movement of pollutants. At Ailaoshan in Yunnan province (Zhang et al.,
290 2016a), a higher TGM concentration during the ISM period ($2.22 \pm 0.58 \text{ ng m}^{-3}$) than
291 the PISM period ($1.99 \pm 0.66 \text{ ng m}^{-3}$) was also observed. The TGM concentration
292 during the ISM period ($2.00 \pm 0.77 \text{ ng m}^{-3}$) was also higher than that during the PISM
293 period ($1.83 \pm 0.78 \text{ ng m}^{-3}$) at Waliguan station in the northeastern Tibetan Plateau (Fu
294 et al., 2012a). In contrast to GEM, the GOM and PBM levels during the ISM period
295 were lower than the monitored values during the PISM period (Figure S2 and Table 2).
296 In previous studies, the PBM concentration in the Kathmandu Valley was lower
297 during the monsoon period (with a value of $120.5 \pm 105.9 \text{ pg m}^{-3}$) than the
298 pre-monsoon (with a value of $1855.4 \pm 780.8 \text{ pg m}^{-3}$) and post-monsoon periods (with
299 a value of $237.6 \pm 199.4 \text{ pg m}^{-3}$) (Guo et al., 2017). In India, PBM concentrations
300 during the monsoon period (with a value of $158 \pm 34 \text{ pg m}^{-3}$) were lower than that in
301 the non-monsoon season (with a value of $231 \pm 51 \text{ pg m}^{-3}$) (Das et al., 2016). This fact
302 could be possibly attributed to precipitation increases brought by the monsoon, which
303 further causes the wet depositions of PBM from atmosphere. During the ISM period,
304 the precipitation could increase up to 25% in the South Asia and Tibetan Plateau (Ji et
305 al., 2011).

306 **3.2 Diurnal variations of atmospheric Hg species in QNNP**

307 During the PISM period, all the atmospheric Hg species showed clear diurnal
308 patterns (Figure 3). For GEM, the minimum concentrations usually occurred at ~12
309 p.m. (0.87 ng m^{-3} , UTC +6 time), while maximum values occurred before dawn (1.98
310 ng m^{-3} at ~5:30 a.m.). From the afternoon, GEM concentration increased consistently
311 and reached a peak at sunrise (with a value of 1.98 ng m^{-3}). Unlike the daily GEM
312 changes, GOM and PBM concentrations usually reached maximum concentrations
313 from ~10:00 a.m. to ~4:00 p.m. in the day, and the concentrations remained relative
314 stable for the rest of the day. During the ISM period, the diurnal variation of
315 atmospheric Hg species was less significant compared to the values in the PISM
316 period. At different stages of the ISM period, the diurnal pattern was also different.



317 The GEM diurnal variation value decreased over time, from 1.03 ng m^{-3} during the
318 initial ISM period to 0.43 ng m^{-3} during the final ISM period. For GEM
319 concentrations during the ISM period, the minimum values all occurred at $\sim 2:00$ p.m.,
320 and the maximum values were observed at $\sim 6:00$ a.m. After the sunrise, GEM
321 concentrations decreased continuously to lower values at noon.

322 Compared with daily GEM changes in previous studies, the diurnal tendency in
323 QNNP is unique (shown in Table 2). For the sampling sites in other studies, the
324 highest GEM concentrations were usually observed during the daytime (Fu et al.,
325 2008; Mukherjee et al., 2009; Nair et al., 2012; Jen et al., 2014; Karthik et al., 2017).
326 Kellerhals et al. (2003) reported that the majority of monitoring sites in CAMNet have
327 a common pattern with the maximum concentration around noon and the minimum
328 concentration before sunrise. Compared to other observation stations and considering
329 QNNP as a remote region with high altitude, sparse population and rare industries, the
330 observed result here may indicate a simple mechanism of variation in GEM
331 concentration without the complex effect of human activities. Previous studies
332 suggested that the planetary boundary layer (PBL) could have significant effects on
333 the concentrations of atmospheric pollutants near the ground (Tie et al., 2007; Han et
334 al., 2009; Quan et al., 2013). With a large glacier coverage ($\sim 2,710 \text{ km}^2$), the structure
335 of the boundary layer over QNNP was significantly affected by glacier winds (Li et al.,
336 2006). The local PBL may be subject to impacts from the glacier-covered
337 environment and have a significant diurnal variation. Following sunrise, with the
338 strengthening of the glacier wind, a strong convection current starts to grow in the
339 troposphere, and the stock of GEM in the near-ground atmosphere is depleted quickly,
340 leading to the quick decrease in concentrations. In contrast, after sunset, with the
341 weakening of the glacier wind, the nocturnal stable boundary layer takes a dominate
342 position controlling the surface layer, and its height is relatively low (Li et al., 2006),
343 leading to the accumulation of GEM concentrations.

344 Comparing the diurnal variations between the PISM and ISM period, the
345 atmospheric Hg concentrations have almost the same pattern of variations, but the



346 variation during the ISM period is relatively lower, and the variation becomes less
347 significant in the later stages of the ISM (Figure 3). The GEM concentration usually
348 peaked at ~5 a.m. - 6 a.m. in both the PISM and ISM periods. While the peak GEM
349 concentrations were almost at the same level in the whole period, the decreasing
350 diurnal variations were mainly due to the increasing GEM concentrations in the
351 afternoon. The increased GEM concentrations in the afternoon may indicate new
352 GEM sources in the ISM period. One possible source of GEM in the afternoon might
353 be Hg(0) reemission from the glaciers. Holmes et al. (2010) reported that
354 snow-covered land could be a reservoir for the conversion of oxidized Hg to GEM
355 under the sunlight, and approximately 60% of the Hg deposited to snow cover would
356 eventually be reemitted to the air. A shorter reservoir lifetime for deposited Hg in
357 snowpack was also reported when temperature rises (Faň et al., 2007). With the
358 increases of ambient temperature and radiation from April to August, the reemission
359 of GEM from the glaciers could increase as well. As the snow coverage in the QNNP
360 decreased significantly from the PISM to ISM period (Figure S3), some of the
361 released Hg may become new GEM sources from the initial ISM to the final stage of
362 the ISM period. More GEM was released due to the higher temperature and stronger
363 radiation in afternoon.

364 **3.3 Source identification for atmospheric Hg in the QNNP**

365 **3.3.1 Wind direction dependence of Hg concentrations**

366 Figure 4 shows the concentration roses of GEM, GOM and PBM at the sampling
367 site during the PISM and ISM period, respectively. All concentrations of the three
368 species have a strong dependence on the wind directions. During the PISM period, the
369 predominant wind directions with Hg masses are northeast and southwest. Wind from
370 the northeast of QNNP originates from and/or passes through other parts of China.
371 The southwest wind, which is the dominant direction and contains the largest amount
372 of Hg, potentially brought air masses from India and Nepal to QNNP. During the ISM
373 period, the predominant wind directions with Hg changed to the south and northeast.
374 Considering the transport rates of species Hg concentrations (length of sector) from



375 different directions, both directions may have greatly contributed to the Hg
376 concentration in QNNP, while the air masses from south brought relatively larger
377 amounts of GOM and PBM.

378 Relatively low GEM concentrations ($<1.5 \text{ ng m}^{-3}$) were observed in most of the
379 samples (80.0%) of air masses in the predominant Hg-transport direction (from
380 southwest to west) during the PISM period, which is due to the control of westerlies.
381 With high wind speed (Table 1) and coming from Central Asia, the westerlies are the
382 predominant wind containing low pollutant levels that spread in the QNNP during the
383 PISM period (Kotlia et al., 2015). Relatively high GEM concentrations ($>1.5 \text{ ng m}^{-3}$)
384 were found in 92.4% of the samples for the predominant Hg direction during the ISM
385 period under the control of the monsoon (Kotlia et al., 2015), which might indicate
386 that the transported air masses are coming from polluted regions. GOM and PBM had
387 similar patterns under the control of the westerlies and monsoon during the PISM and
388 ISM period, respectively.

389 **3.3.2 Air mass back trajectories analysis**

390 To further quantify the contributions of different sources to GEM concentrations,
391 an air mass back trajectory simulation and trajectory cluster analyses were applied in
392 this study. Figure 5 provides the trajectory clusters of GEM during the PISM and ISM
393 periods. According to the total spatial variation index, all the trajectories were
394 grouped into 6 clusters. During the PISM period (Figure 5a), GEM concentration
395 from cluster 3 (with the frequency of 17%) was the highest (1.36 ng m^{-3}), which
396 originated from or passed through central Asia, northern India and northwestern Nepal.
397 Cluster 2 (14%), cluster 5 (19%) and cluster 6 (19%) represent the air masses that
398 pass through northern India and northwestern Nepal. According to the local Hg
399 emission inventory (UNEP, 2013), Hg in this air mass most likely originated from
400 central Pakistan and northern India. Cluster 4 (29%) represents the air masses that
401 originated from or passed through different cities in northern India. Based on the
402 previous atmospheric Hg emission inventories (UNEP, 2013; Simone et al., 2016), Hg
403 emission in the west Asia and central Asia is not significant. Based on a combination



404 of the pathway analysis, emission inventory and GEM concentration during the PISM
405 period, almost all the GEM delivered by air masses to QNNP was from northern India
406 and passed through Nepal.

407 During the ISM period (Figure 5b-5f), the transport pathways of atmospheric Hg
408 changed signally with the monsoon onset process of the ISM and differed strongly
409 from the PISM period. During the ISM1 period (Figure 5b), the onset of the ISM was
410 under development, leading to the scattered clusters. GEM levels in cluster 3 (21%)
411 were the highest (1.51 ng m^{-3}), which originated from or passed through the Tibetan
412 Plateau. Cluster 4 (13%), cluster 2 (17%) and cluster 6 (38%) represent the pollutant
413 coming from Nepal, and the trajectory is relatively short. During the ISM2 period, all
414 the clusters originated from or passed through central Asia, northern India and
415 northwestern Nepal (Figure 5c). The clusters were similar to most of the clusters
416 during the PISM period; however, the GEM concentrations in these clusters were
417 higher than those during the PISM period. During the ISM3 period (Figure 5d), most
418 of the clusters moved from west to south of QNNP. Cluster 2 (1.56 ng m^{-3} , 44%)
419 represents the pollutant coming from Bangladesh and passing through southeastern
420 Nepal. Cluster 3 (1.62 ng m^{-3} , 33%) originated from or passed through central Nepal.
421 The share of air masses coming from central Asia, northern India and northwestern
422 Nepal dropped to approximately 22%. During the ISM4 period (Figure 5e), the
423 clusters moved further west to Bangladesh and eastern India. Except for cluster 4
424 (6%), the other clusters originated from or passed through Bangladesh, eastern India
425 and northeastern Nepal. The condition during the ISM5 period was almost the same as
426 the ISM4 period: pollutants were coming from Bangladesh and eastern India and
427 passed through southeastern Nepal.

428 PSCF models were also applied to identify the potential sources by combining the
429 backward trajectory simulation and Hg monitoring concentrations. Figure 6 shows the
430 regional contributions of GEM emission sources during the PISM period and ISM
431 period (ISM1-5). During the PISM period (Figure 6a), most of the Hg sources were in
432 Pakistan, northern India and central Nepal (Zhang et al., 2015a). The QNNP was most



433 likely impacted by the Hg emissions in Karachi, Lahore (Pakistan), New Delhi, Uttar
434 Pradesh (India), Katmandu and Pokhara (Nepal), all of which are large urban regions
435 with intensive industrial activities. With the development of the ISM, the potential
436 sources gradually shifted from western Nepal to eastern Nepal and Bangladesh
437 (Figure 6b-f). The PSCF analysis indicated that the air masses could have
438 transboundary transport events from Pakistan, India, Nepal and Bangladesh to QNNP.

439 Atmospheric Hg clusters during both the PISM and ISM periods indicated that the
440 air masses, which originated from or passed through northern India and Nepal, would
441 make great contributions to the Hg concentration in the QNNP. Northern India and
442 Nepal were also identified as potential source regions for QNNP. Clusters 2-6 of the
443 PISM period represent the air masses from outside China, and they show that over 97%
444 of the GEM in QNNP was transported from outside China during the PISM period.
445 During ISM2-5 the period, over 95% of the GEM was transported to QNNP from
446 outside China. Meanwhile, the GEM concentration increased by 10% from the PISM
447 to ISM period according to the site monitoring data, indicating the increasing amount
448 of transported GEM. According to the UNEP Hg emission inventory (UNEP, 2013),
449 northern India is an important Hg source which might be responsible for the
450 trans-boundary transportation of Hg to China (Figure 5), and the growing emissions in
451 India are related to the rapidly growing economy and increasing usage of fossil fuels
452 (Sharma, 2003). Considering the heavy air pollution in Nepal (Forouzanfar et al.,
453 2015; Rupakheti et al., 2017), Nepal might be an underestimated Hg source in the
454 modeling and should be taken into consideration in further work.

455 Under the control of the ISM during the ISM2 period, the high PBM concentration
456 may be related to the biomass burning in the source region. According to the PSCF
457 analysis, northern India and Nepal are the potential source regions during the ISM2
458 period. The source identification by back trajectory simulation and trajectory cluster
459 analyses also indicated that northern India and Nepal are in the air mass transport
460 trajectory that would transport Hg to QNNP. Finley et al. (2009) reported that PBM
461 concentrations may associated with Hg emissions from wildfire events. One possible



462 cause of the observed high PBM concentration is the frequent fire events that
463 occurred during the ISM2 period in the air masses trajectory. Figure S3 shows the fire
464 hotspots observed by MODIS from April to August 2016. During the ISM2 period,
465 frequent fire hotspots were identified in the source region, and large amounts of PBM
466 were released into the atmosphere from biomass burning. The transport of those air
467 masses with enriched PBM was controlled by the ISM and intensified by glacier
468 winds. The transport of polluted air to QNNP resulted in the outburst of PBM
469 concentration during the ISM2 period. During the PISM period, although the number
470 of fire hotspots was much higher, most of the fire hotspots locations were not in the
471 potential source region (Figure 6a and Figure S4), resulting in the low GOM and
472 PBM concentrations observed.

473 **3.4 Implications from this study**

474 At a high altitude and located in the deep southern Tibetan Plateau, QNNP is
475 isolated from anthropogenic perturbations and industrial activities, and this area was
476 thought to be shielded from pollutant inputs from South Asia. However, our results
477 show that the Hg concentration in this region is not as low as previously expected.
478 During the whole monitoring period, the highest GEM concentration reached 3.74 ng
479 m⁻³, ~2.5 times higher than the average concentration in the Northern Hemisphere
480 (~1.5-1.7 ng m⁻³) (Lindberg et al., 2007; Slemr et al., 2015; Venter et al., 2015). The
481 average GEM concentration in the middle stage of the ISM was 1.56 ng m⁻³, which is
482 inside the average range of observed Northern Hemisphere GEM concentrations.
483 Even considering the PISM period, which is a period of relatively lower GEM levels
484 in QNNP, the average GEM concentration (1.31±0.42 ng m⁻³) was at the same level
485 as some monitoring stations in the Northern Hemisphere (e.g., 1.35±0.17 ng m⁻³ in a
486 rural site in Atlanta, USA).

487 We now recognize that trans-boundary transportation is an important mechanism
488 that can influence Hg distribution in this region. In particular, the air masses
489 transported to QNNP might be primary under the control of mesoscale ISM drivers
490 and intensified by regional glacier winds (Figure 7). From the PISM to ISM periods,



491 the warm center gradually shifts northwestward from low latitudes to the QNNP
492 (Wang et al., 2001; Ge et al., 2017), and the South Asian High moves onto the
493 Tibetan Plateau and maintains a strong upper-level divergence and upward motion.
494 The upward motion makes the air masses cross the high-altitude Himalayan
495 mountains and move to mainland China (Xu et al., 2009; Bonasoni et al., 2010). The
496 transboundary transported air masses can be pumped down right after crossing Mt.
497 Qomolangma due to the control of the regionally unique wind transportation mode,
498 the glacier wind. Hence, in addition to the monsoon, the trans-boundary transport of
499 Hg could also be intensified by regional glacier winds, leading to the increases of
500 atmospheric Hg in this region. As in other studies in the northern or eastern Tibetan
501 Plateau, the glacier wind can pump down air masses from stratosphere to the surface
502 in QNNP (Cai et al., 2007). The pump movement is remarkably efficient at
503 transporting air masses (Lelieveld et al., 2018), bringing a considerable amount of
504 pollutants to QNNP.

505 In 2013, the Minamata Convention on Mercury was developed to control global Hg
506 pollution (Minamata Convention on Mercury). Atmosphere Hg has been reported
507 (Zhang et al., 2016b) to have strongly declined ($\sim 1\text{--}2\% \text{ y}^{-1}$). Under the Convention, a
508 National Implementation Plan on Mercury Control has also been developed in China
509 to fulfill the commitment to control and reduce Hg emissions (World Bank, 2016).
510 GEM concentrations in East China decreased from $2.68 \pm 1.07 \text{ ng m}^{-3}$ in 2014 to
511 $1.60 \pm 0.56 \text{ ng m}^{-3}$ in 2016 (Tang et al., 2018). However, the source identity analysis in
512 QNNP indicates that foreign regions of China were the main contributor responsible
513 for the observed pollutants (accounting for 95% of the whole trajectory during the
514 main ISM period). This result indicates that the Hg concentration in QNNP could
515 hardly benefit from China's efforts toward Hg reductions. South Asian developing
516 countries (e.g., India, Nepal, and Bangladesh) (Streets et al., 2011; Zhang et al., 2015b;
517 Yang et al., 2018) should be the key to controlling atmospheric Hg concentrations in
518 QNNP. Hg emissions in India were estimated to be approximately 310 tons in 2010
519 and are predicted to rise to 540 tons in 2020 (Burger Chakraborty et al., 2013). It is



520 urgent for those countries to take immediate actions to reduce Hg emissions, which is
521 crucial to reduce the atmospheric Hg concentrations in QNNP.

522 **4. Conclusions**

523 A comprehensive investigation of the concentrations, origin and transport of GEM,
524 GOM and PBM was made in QNNP, a remote, high-altitude station located at the
525 boundary between the Indian subcontinent and the Tibetan Plateau and in the transport
526 pathway of the ISM from South Asia to the Tibetan Plateau. The average GEM
527 concentration ($1.31 \pm 0.42 \text{ ng m}^{-3}$) during the PISM period was lower than that
528 ($1.44 \pm 0.36 \text{ ng m}^{-3}$) during the ISM period. The average GOM and PBM
529 concentrations during the PISM period were higher than those during the ISM period,
530 which might be related to the increasing wet depositions during the ISM period. The
531 average GOM concentration was higher than in most rural areas in the US and China.
532 The GEM concentration had a significant diurnal variation pattern in QNNP, with the
533 maximum GEM concentration observed before sunrise and a sharp decrease after
534 sunrise until noon. The range of the diurnal variation declined from April to August,
535 which could be related to the re-emission of Hg from snow cover and melted snow.

536 According to the backward trajectory analysis and cluster analysis, most of the air
537 masses with high GEM concentrations in QNNP originated from or passed through
538 Bangladesh, northern India and central Nepal. With the PSCF analysis, we found that
539 Pakistan, northern India and Nepal are potential source regions during the PISM
540 period, and Bangladesh, north India, Nepal were identified as outbound potential
541 sources during the ISM period. During the ISM period, the air masses would cross the
542 high-altitude Himalayan mountains with the help of the ISM. Once the air masses
543 passed through Himalaya, they could be trapped in the surface layer and transported
544 to QNNP by the all-day-long downslope glacier wind. It should be noted that the
545 atmospheric Hg values in QNNP were contaminated and even higher than the
546 reported values in some background regions. Because Hg is easily transported long
547 distances via the atmosphere, the nations in South Asia must work together to develop
548 and apply appropriate pollutant-reduction strategies to reduce Hg emission.

549 **Acknowledgments**

550 This study was funded by the National Natural Science Foundation of China (Grant
551 #41630748, 41501517, 41571130010) and the Natural Science Foundation of Tianjin
552 (Grant #16JCQNJC08300). The authors are grateful to NOAA for providing the
553 HYSPLIT model and GFS meteorological files, to NASA for providing the MODIS
554 files. We also thank the staffs of the Atmospheric and Environmental Comprehensive
555 Observation and Research Station of Chinese Academy of Sciences on Mt.
556 Qomolangma for field sampling assistance.

557 **References**

- 558 Angot, H., Dion, I., Vogel, N., Legrand, M., Magand, O., and Dommergue, A.: Multi-year record of
559 atmospheric mercury at Dumont d'Urville, East Antarctic coast: continental outflow and oceanic
560 influences, *Atmos. Chem. Phys.*, 16, 8265-8279, 2016.
- 561 Ashbaugh, L. L., Malm, W. C., and Sadeh, W. Z.: A residence time probability analysis of sulfur
562 concentrations at Grand Canyon National Park, *Atmospheric Environment* (1967), 19, 1263-1270,
563 1985.
- 564 Bolch, T., Kulkarni, A., Kääb, A., Huggel, C., Paul, F., Cogley, J., Frey, H., Kargel, J. S., Fujita, K., and
565 Scheel, M.: The state and fate of Himalayan glaciers, *Science*, 336, 310-314, 2012.
- 566 Cai, X., Song, Y., Zhu, T., Lin, W., and Kang, L.: Glacier winds in the Rongbuk Valley, north of Mount
567 Everest: 2. Their role in vertical exchange processes, *J. Geo. Res. Atmos.*, 112, 2007.
- 568 Chai, T., Stein, A., Ngan, F., and Draxler, R.: Inverse modeling with HYSPLIT Lagrangian Dispersion
569 Model-Tests and Evaluation using the Cross Appalachian Tracer Experiment (CAPTEX) data, *AGUFM*,
570 2016,
- 571 Chai, T., Crawford, A., Stunder, B., Pavolonis, M. J., Draxler, R., and Stein, A.: Improving volcanic ash
572 predictions with the HYSPLIT dispersion model by assimilating MODIS satellite retrievals, *Atmos.*
573 *Chem. Phys.*, 17, 2865-2879, 2017.
- 574 Chen, G., Li, J., Chen, B., Wen, C., Yang, Q., Alsaedi, A., and Hayat, T.: An overview of mercury
575 emissions by global fuel combustion: the impact of international trade, *Renewable and Sustainable*
576 *Energy Reviews*, 65, 345-355, 2016.
- 577 Das, R., Wang, X., Khezri, B., Webster, R. D., Sikdar, P. K., and Datta, S.: Mercury isotopes of
578 atmospheric particle bound mercury for source apportionment study in urban Kolkata, India, *Elem Sci*
579 *Anth*, 4, 2016.
- 580 de Foy, B., Tong, Y., Yin, X., Zhang, W., Kang, S., Zhang, Q., Zhang, G., Wang, X., and Schauer, J. J.:
581 First field-based atmospheric observation of the reduction of reactive mercury driven by sunlight,
582 *Atmos. Environ.*, 134, 7e39, 2016.
- 583 Ebinghaus, R., Kock, H., Coggins, A., Spain, T., Jennings, S., and Temme, C.: Long-term



- 584 measurements of atmospheric mercury at Mace Head, Irish west coast, between 1995 and 2001, Atmos.
585 Environ., 36, 5267-5276, 2002.
- 586 Fa ñ, X., Grangeon, S., Bahlmann, E., Fritsche, J., Obrist, D., Dommergue, A., Ferrari, C. P., Cairns, W.,
587 Ebinghaus, R., and Barbante, C.: Diurnal production of gaseous mercury in the alpine snowpack before
588 snowmelt, J. Geo. Res. Atoms., 112, 2007.
- 589 Fa ñ, X., Obrist, D., Hallar, A. G., McCubbin, I., and Rahn, T.: High levels of reactive gaseous mercury
590 observed at a high elevation research laboratory in the Rocky Mountains, Atmos. Chem. Phys., 9,
591 8049-8060,'D'O'I:' 10.5194/acp-9-8049-2009, 2009.
- 592 Fang, G.-C., Wu, Y.-S., and Chang, T.-H.: Comparison of atmospheric mercury (Hg) among Korea,
593 Japan, China and Taiwan during 2000–2008, J. Hazard. Mater., 162, 607-615, 2009.
- 594 Finley, B., Swartzendruber, P., and Jaffe, D.: Particulate mercury emissions in regional wildfire plumes
595 observed at the Mount Bachelor Observatory, Atmos. Environ., 43, 6074-6083, 2009.
- 596 Forouzanfar, M. H., Alexander, L., Anderson, H. R., Bachman, V. F., Biryukov, S., Brauer, M., Burnett,
597 R., Casey, D., Coates, M. M., and Cohen, A.: Global, regional, and national comparative risk
598 assessment of 79 behavioural, environmental and occupational, and metabolic risks or clusters of risks
599 in 188 countries, 1990–2013: a systematic analysis for the Global Burden of Disease Study 2013, The
600 Lancet, 386, 2287-2323, 2015.
- 601 Fu, X., Feng, X., Zhu, W., Wang, S., and Lu, J.: Total gaseous mercury concentrations in ambient air in
602 the eastern slope of Mt. Gongga, South-Eastern fringe of the Tibetan plateau, China, Atmos. Environ.,
603 42, 970-979, 2008.
- 604 Fu, X., Feng, X., Dong, Z., Yin, R., Wang, J., Yang, Z., and Zhang, H.: Atmospheric gaseous elemental
605 mercury (GEM) concentrations and mercury depositions at a high-altitude mountain peak in south
606 China, Atom. Chem. Phys., 10, 2425-2437, 2010.
- 607 Fu, X., Feng, X., Liang, P., Zhang, H., Ji, J., and Liu, P.: Temporal trend and sources of speciated
608 atmospheric mercury at Waliguan GAW station, Northwestern China, Atom. Chem. Phys., 12,
609 1951-1964, 2012a.
- 610 Fu, X., Feng, X., Shang, L., Wang, S., and Zhang, H.: Two years of measurements of atmospheric total
611 gaseous mercury (TGM) at a remote site in Mt. Changbai area, Northeastern China, Atom. Chem. Phys.,
612 12, 4215-4226, 2012b.
- 613 Gay, D. A., Schmeltz, D., Prestbo, E., Olson, M., Sharac, T., and Tordon, R.: The Atmospheric Mercury
614 Network: measurement and initial examination of an ongoing atmospheric mercury record across North
615 America, Atmospheric Chemistry and Physics, 13, 11339-11349,'D'O'I:' 10.5194/acp-13-11339-2013,
616 2013.
- 617 Ge, J., You, Q., and Zhang, Y.: The influence of the Asian summer monsoon onset on the northward
618 movement of the South Asian high towards the Tibetan Plateau and its thermodynamic mechanism,
619 IJCLI, 2017.
- 620 Global, B. P.: BP statistical review of world energy June 2018, em:
621 <http://www.bp.com/en/global/corporate/energy-economics/statistical-review-of-world-energy.html>,



- 622 2018.
- 623 Gratz, L., Esposito, G., Dalla Torre, S., Cofone, F., Pirrone, N., and Sprovieri, F.: First Measurements
624 of Ambient Total Gaseous Mercury (TGM) at the EvK2CNR Pyramid Observatory in Nepal, E3S Web
625 of Conferences, 2013,
- 626 Guo, J., Kang, S., Huang, J., Zhang, Q., Rupakheti, M., Sun, S., Tripathee, L., Rupakheti, D., Panday,
627 A. K., and Sillanpää M.: Characterizations of atmospheric particulate-bound mercury in the
628 Kathmandu Valley of Nepal, South Asia, *Sci. Total Environ.*, 579, 1240-1248, 2017.
- 629 Han, S., Bian, H., Tie, X., Xie, Y., Sun, M., and Liu, A.: Impact of nocturnal planetary boundary layer
630 on urban air pollutants: Measurements from a 250-m tower over Tianjin, China, *J. Hazard. Mater.*, 162,
631 264-269, 2009.
- 632 Holmes, C. D., Jacob, D. J., Corbitt, E. S., Mao, J., Yang, X., Talbot, R., and Slemr, F.: Global
633 atmospheric model for mercury including oxidation by bromine atoms, *Atmos. Chem. Phys.*, 10,
634 12037-12057, 2010.
- 635 Huang, J., Lyman, S. N., Hartman, J. S., and Gustin, M. S.: A review of passive sampling systems for
636 ambient air mercury measurements, *Environmental science. Processes & impacts*, 16, 374-392, DOI:
637 10.1039/c3em00501a, 2014.
- 638 Hurst, T., and Davis, C.: Forecasting volcanic ash deposition using HYSPLIT, *Journal of Applied*
639 *Volcanology*, 6, 5, 2017.
- 640 Jen, Y.-H., Chen, W.-H., Hung, C.-H., Yuan, C.-S., and Ie, I.-R.: Field measurement of total gaseous
641 mercury and its correlation with meteorological parameters and criteria air pollutants at a coastal site of
642 the Penghu Islands, *Aerosol Air Qual. Res.*, 14, 364-375, 2014.
- 643 Ji, Z., Kang, S., Zhang, D., Zhu, C., Wu, J., and Xu, Y.: Simulation of the anthropogenic aerosols over
644 South Asia and their effects on Indian summer monsoon, *CLDy*, 36, 1633-1647, 2011.
- 645 Kaiser, A., Scheifinger, H., Spangl, W., Weiss, A., Gilge, S., Fricke, W., Ries, L., Cemas, D., and
646 Jesenovec, B.: Transport of nitrogen oxides, carbon monoxide and ozone to the alpine global
647 atmosphere watch stations Jungfrauoch (Switzerland), Zugspitze and Hohenpeißenberg (Germany),
648 Sonnblick (Austria) and Mt. Kravec (Slovenia), *Atmos. Environ.*, 41, 9273-9287, 2007.
- 649 Karthik, R., Paneerselvam, A., Ganguly, D., Hariharan, G., Srinivasalu, S., Purvaja, R., and Ramesh, R.:
650 Temporal variability of atmospheric Total Gaseous Mercury and its correlation with meteorological
651 parameters at a high-altitude station of the South India, *Atmospheric Pollution Research*, 8, 164-173,
652 2017.
- 653 Kellerhals, M., Beauchamp, S., Belzer, W., Blanchard, P., Froude, F., Harvey, B., McDonald, K., Pilote,
654 M., Poissant, L., and Puckett, K.: Temporal and spatial variability of total gaseous mercury in Canada:
655 results from the Canadian Atmospheric Mercury Measurement Network (CAMNet), *Atmos. Environ.*,
656 37, 1003-1011, 2003.
- 657 Kim, E., Hopke, P. K., Kenski, D. M., and Koerber, M.: Sources of fine particles in a rural midwestern
658 US area, *Environ. Sci. Technol.*, 39, 4953-4960, 2005.
- 659 Kotlia, B. S., Singh, A. K., Joshi, L. M., and Dhaila, B. S.: Precipitation variability in the Indian



- 660 Central Himalaya during last ca. 4,000 years inferred from a speleothem record: Impact of Indian
661 Summer Monsoon (ISM) and Westerlies, *Quaternary International*, 371, 244-253, 2015.
- 662 Landis, M. S., Stevens, R. K., Schaedlich, F., and Prestbo, E. M.: Development and characterization of
663 an annular denuder methodology for the measurement of divalent inorganic reactive gaseous mercury
664 in ambient air, *Environmental science & technology*, 36, 3000-3009, 2002.
- 665 Lelieveld, J., Bourtsoukidis, E., Brühl, C., Fischer, H., Fuchs, H., Harder, H., Hofzumahaus, A.,
666 Holland, F., Marno, D., and Neumaier, M.: The South Asian monsoon—Pollution pump and purifier,
667 *Science*, eaar2501, 2018.
- 668 Li, C., Bosch, C., Kang, S., Andersson, A., Chen, P., Zhang, Q., Cong, Z., Chen, B., Qin, D., and
669 Gustafsson, Ö.: Sources of black carbon to the Himalayan–Tibetan Plateau glaciers, *Nature*
670 *Communications*, 7, 12574, 2016.
- 671 Li, M., Dai, Y., Ma, Y., Zhong, L., and Lu, S.: Analysis on structure of atmospheric boundary layer and
672 energy exchange of surface layer over Mount Qomolangma region, *Plateau Meteorology*, 25, 807-813,
673 2006.
- 674 Lindberg, S., Bullock, R., Ebinghaus, R., Engstrom, D., Feng, X., Fitzgerald, W., Pirrone, N., Prestbo,
675 E., and Seigneur, C.: A synthesis of progress and uncertainties in attributing the sources of mercury in
676 deposition, *AMBIO: a Journal of the Human Environment*, 36, 19-33, 2007.
- 677 Lindberg, S. a., and Stratton, W.: Atmospheric mercury speciation: concentrations and behavior of
678 reactive gaseous mercury in ambient air, *Environmental Science & Technology*, 32, 49-57, 1998.
- 679 Lynam, M. M., Dvonch, J. T., Hall, N. L., Morishita, M., and Barres, J. A.: Spatial patterns in wet and
680 dry deposition of atmospheric mercury and trace elements in central Illinois, USA, *Environmental*
681 *Science and Pollution Research*, 21, 4032-4043, 2014.
- 682 Mukherjee, A. B., Bhattacharya, P., Sarkar, A., and Zevenhoven, R.: Mercury emissions from industrial
683 sources in India and its effects in the environment, in: *Mercury Fate and Transport in the Global*
684 *Atmosphere*, Springer, 81-112, 2009.
- 685 Nair, U. S., Wu, Y., Walters, J., Jansen, J., and Edgerton, E. S.: Diurnal and seasonal variation of
686 mercury species at coastal-suburban, urban, and rural sites in the southeastern United States,
687 *Atmospheric environment*, 47, 499-508, 2012.
- 688 Nie, Y., Zhang, Y., Liu, L., and Zhang, J.: Monitoring glacier change based on remote sensing in the Mt.
689 Qomolangma National Nature Preserve, 1976–2006, *Acta Geographica Sinica*, 65, 13-28, 2010.
- 690 Panthi, J., Dahal, P., Shrestha, M. L., Aryal, S., Krakauer, N. Y., Pradhanang, S. M., Lakhankar, T., Jha,
691 A. K., Sharma, M., and Karki, R.: Spatial and temporal variability of rainfall in the Gandaki River
692 Basin of Nepal Himalaya, *Climate*, 3, 210-226, 2015.
- 693 Pokhrel, B., Gong, P., Wang, X., Gao, S., Wang, C., and Yao, T.: Sources and environmental processes
694 of polycyclic aromatic hydrocarbons and mercury along a southern slope of the Central Himalayas,
695 *Nepal, Environ. Sci. Pollut. Res.*, 23, 13843-13852, 2016.
- 696 Polissar, A., Hopke, P., Paatero, P., Kaufmann, Y., Hall, D., Bodhaine, B., Dutton, E., and Harris, J.:
697 The aerosol at Barrow, Alaska: long-term trends and source locations, *Atmos. Environ.*, 33, 2441-2458,



- 698 1999.
- 699 Qiu, J.: China: the third pole, *Nature News*, 454, 393-396, 2008.
- 700 Quan, J., Gao, Y., Zhang, Q., Tie, X., Cao, J., Han, S., Meng, J., Chen, P., and Zhao, D.: Evolution of
701 planetary boundary layer under different weather conditions, and its impact on aerosol concentrations,
702 *Particuology*, 11, 34-40, 2013.
- 703 Rupakheti, D., Adhikary, B., Praveen, P. S., Rupakheti, M., Kang, S., Mahata, K. S., Naja, M., Zhang,
704 Q., Panday, A. K., and Lawrence, M. G.: Pre-monsoon air quality over Lumbini, a world heritage site
705 along the Himalayan foothills, *Atom. Chem. Phys.*, 17, 11041-11063, 2017.
- 706 Rutter, A. P., Schauer, J. J., Lough, G. C., Snyder, D. C., Kolb, C. J., Von Klooster, S., Rudolf, T.,
707 Manolopoulos, H., and Olson, M. L.: A comparison of speciated atmospheric mercury at an urban
708 center and an upwind rural location, *Journal of Environmental Monitoring*, 10, 102-108, 2008.
- 709 Seigneur, C., Vijayaraghavan, K., and Lohman, K.: Atmospheric mercury chemistry: Sensitivity of
710 global model simulations to chemical reactions, *Journal of Geophysical Research: Atmospheres*, 111,
711 2006.
- 712 Simone, F. D., Gencarelli, C. N., Hedgecock, I. M., and Pirrone, N.: A modeling comparison of
713 mercury deposition from current anthropogenic mercury emission inventories, *Environ. Sci. Technol.*,
714 50, 5154-5162, 2016.
- 715 Slemr, F., Angot, H., Dommergue, A., Magand, O., Barret, M., Weigelt, A., Ebinghaus, R., Brunke,
716 E.-G., Pfaffhuber, K. A., and Edwards, G.: Comparison of mercury concentrations measured at several
717 sites in the Southern Hemisphere, *Atmospheric Chemistry and Physics*, 15, 3125-3133, 2015.
- 718 Song, Y., Zhu, T., Cai, X., Lin, W., and Kang, L.: Glacier winds in the Rongbuk Valley, north of Mount
719 Everest: 1. Meteorological modeling with remote sensing data, *J. Geo. Res. Atmos.*, 112, 2007.
- 720 Sprovieri, F., Pirrone, N., Bencardino, M., D'Amore, F., Carbone, F., Cinnirella, S., Mannarino, V.,
721 Landis, M., Ebinghaus, R., and Weigelt, A.: Atmospheric mercury concentrations observed at
722 ground-based monitoring sites globally distributed in the framework of the GMOS network,
723 *Atmospheric Chemistry and Physics*, 16, 11915-11935, 2016.
- 724 Stein, A., Draxler, R. R., Rolph, G. D., Stunder, B. J., Cohen, M., and Ngan, F.: NOAA's HYSPLIT
725 atmospheric transport and dispersion modeling system, *Bulletin of the American Meteorological*
726 *Society*, 96, 2059-2077, 2015.
- 727 Streets, D. G., Devane, M. K., Lu, Z., Bond, T. C., Sunderland, E. M., and Jacob, D. J.: All-time
728 releases of mercury to the atmosphere from human activities, *Environ. Sci. Technol.*, 45, 10485-10491,
729 2011.
- 730 Swartzendruber, P., Jaffe, D., and Finley, B.: Improved fluorescence peak integration in the Tekran
731 2537 for applications with sub-optimal sample loadings, *Atmos. Environ.*, 43, 3648-3651, 2009.
- 732 Tang, Y., Wang, S., Wu, Q., Liu, K., Wang, L., Li, S., Gao, W., Zhang, L., Zheng, H., and Li, Z.: Recent
733 decrease trend of atmospheric mercury concentrations in East China: the influence of anthropogenic
734 emissions, *Atom. Chem. Phys.*, 18, 8279-8291, 2018.
- 735 Tie, X., Madronich, S., Li, G., Ying, Z., Zhang, R., Garcia, A. R., Lee-Taylor, J., and Liu, Y.:



- 736 Characterizations of chemical oxidants in Mexico City: A regional chemical dynamical model
737 (WRF-Chem) study, *Atmos. Environ.*, 41, 1989-2008, 2007.
- 738 UNEP, U. G. M. A.: Sources, Emissions, Releases and Environmental Transport; UNEP Chemicals
739 Branch: Geneva, Switzerland, 2013, There is no corresponding record for this reference, 2013.
- 740 Venter, A., Beukes, J., Van Zyl, P., Brunke, E.-G., Labuschagne, C., Slemr, F., Ebinghaus, R., and Kock,
741 H.: Statistical exploration of gaseous elemental mercury (GEM) measured at Cape Point from 2007 to
742 2011, *Atmospheric Chemistry and Physics*, 15, 10271-10280, 2015.
- 743 Wang, B., Wu, R., and Lau, K.: Interannual variability of the Asian summer monsoon: Contrasts
744 between the Indian and the western North Pacific–East Asian monsoons, *JCLI*, 14, 4073-4090, 2001.
- 745 Wang, C., Wang, X., Gong, P., and Yao, T.: Long-term trends of atmospheric organochlorine pollutants
746 and polycyclic aromatic hydrocarbons over the southeastern Tibetan Plateau, *Sci. Total Environ.*, 624,
747 241-249, 2018.
- 748 Wang, X., Gong, P., Sheng, J., Joswiak, D. R., and Yao, T.: Long-range atmospheric transport of
749 particulate Polycyclic Aromatic Hydrocarbons and the incursion of aerosols to the southeast Tibetan
750 Plateau, *Atmos. Environ.*, 115, 124-131, 2015.
- 751 Ward Jr, J. H.: Hierarchical grouping to optimize an objective function, *Journal of the American*
752 *statistical association*, 58, 236-244, 1963.
- 753 Weiss - Penzias, P., Gustin, M. S., and Lyman, S. N.: Observations of speciated atmospheric mercury at
754 three sites in Nevada: Evidence for a free tropospheric source of reactive gaseous mercury, *J. Geo. Res.*
755 *Atoms.*, 114, 2009.
- 756 World Bank. 2016. *China - Capacity Strengthening for Implementation of Minamata Convention on*
757 *Mercury Project (English)*. Washington, D.C. : World Bank Group.
- 758 Xu, B., Cao, J., Hansen, J., Yao, T., Joswia, D. R., Wang, N., Wu, G., Wang, M., Zhao, H., and Yang,
759 W.: Black soot and the survival of Tibetan glaciers, *Proceedings of the National Academy of Sciences*,
760 106, 22114-22118, 2009.
- 761 Yang, J., Kang, S., Ji, Z., and Chen, D.: Modeling the origin of anthropogenic black carbon and its
762 climatic effect over the Tibetan Plateau and surrounding regions, *J. Geo. Res. Atoms.*, 123, 671-692,
763 2018.
- 764 Zhang, H., Fu, X., Lin, C., Wang, X., and Feng, X.: Observation and analysis of speciated atmospheric
765 mercury in Shangri-La, Tibetan Plateau, China, *Atmos. Chem. Phys.*, 15, 653-665, 2015a.
- 766 Zhang, H., Fu, X., Lin, C.-J., Shang, L., Zhang, Y., Feng, X., and Lin, C.: Monsoon-facilitated
767 characteristics and transport of atmospheric mercury at a high-altitude background site in southwestern
768 China, *ACP*, 16, 2016a.
- 769 Zhang, L., Wang, S., Wang, L., and Hao, J.: Atmospheric mercury concentration and chemical
770 speciation at a rural site in Beijing, China: implications of mercury emission sources, *Atmospheric*
771 *Chemistry and Physics*, 13, 10505-10516, 2013.
- 772 Zhang, R., Wang, H., Qian, Y., Rasch, P. J., Easter, R. C., Ma, P.-L., Singh, B., Huang, J., and Fu, Q.:
773 Quantifying sources, transport, deposition, and radiative forcing of black carbon over the Himalayas



774 and Tibetan Plateau, *Atmos. Chem. Phys.*, 15, 6205-6223, 2015b.
775 Zhang, Y., Jacob, D. J., Horowitz, H. M., Chen, L., Amos, H. M., Krabbenhoft, D. P., Slemr, F., Louis,
776 V. L. S., and Sunderland, E. M.: Observed decrease in atmospheric mercury explained by global
777 decline in anthropogenic emissions, *Proceedings of the National Academy of Sciences*, 113, 526-531,
778 2016b.
779



780 **Figure captions**

781 Figure 1. Location of monitoring site in this study (QNNP);

782 Figure 2. Changes of GEM, GOM and PBM concentrations during the study period;

783 Figure 3. Diurnal variations of GEM, GOM and PBM concentrations during the PISM and ISM
784 period;

785 Figure 4. Concentration roses of GEM, GOM and PBM on different wind directions;

786 Figure 5. Back trajectories analysis at the monitoring site during the PISM period (a) and the ISM
787 period (b-f);

788 Figure 6. Potential source regions and pathways of GEM at monitoring site by the PSCF during
789 the PISM period (a) and the ISM period (b-f);

790 Figure 7. Concept maps for trans-boundary transport of atmospheric Hg

791 **Table captions**

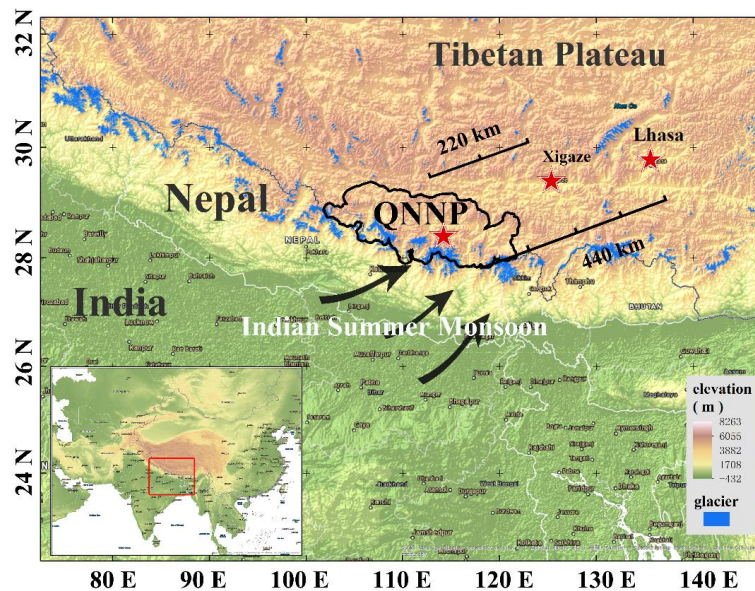
792 Table 1. The statistics of GEM, GOM, PBM and meteorological variables in different episodes at
793 QNNP

794 Table 2. Summary of atmospheric Hg concentration and diurnal variation in previous studies and
795 this study

796



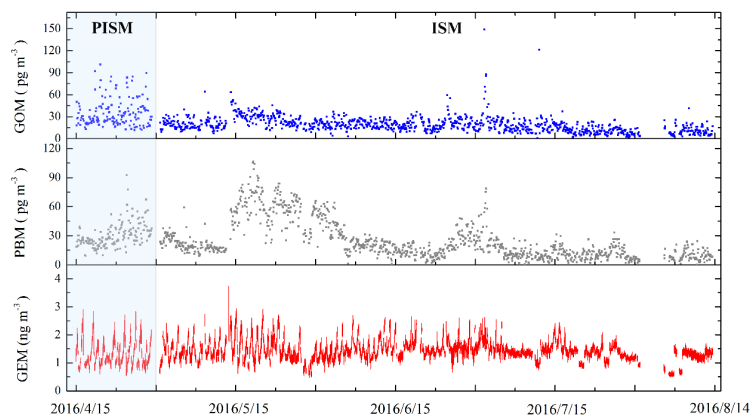
797 **Figure 1**



798



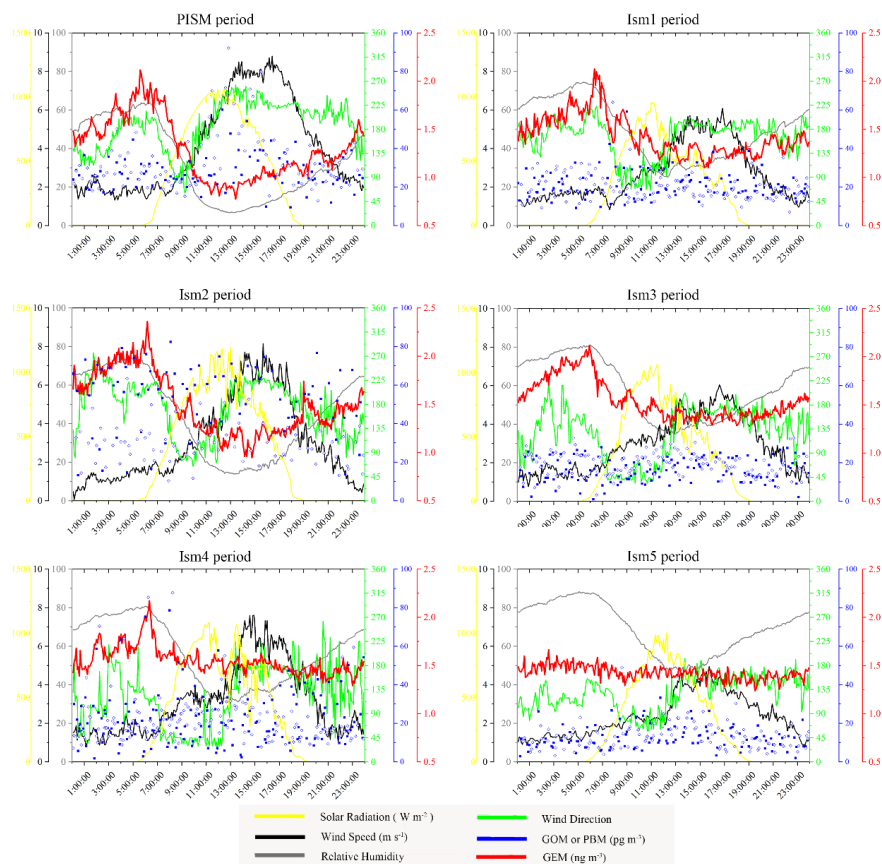
799 **Figure 2**



800
801



802 **Figure 3**

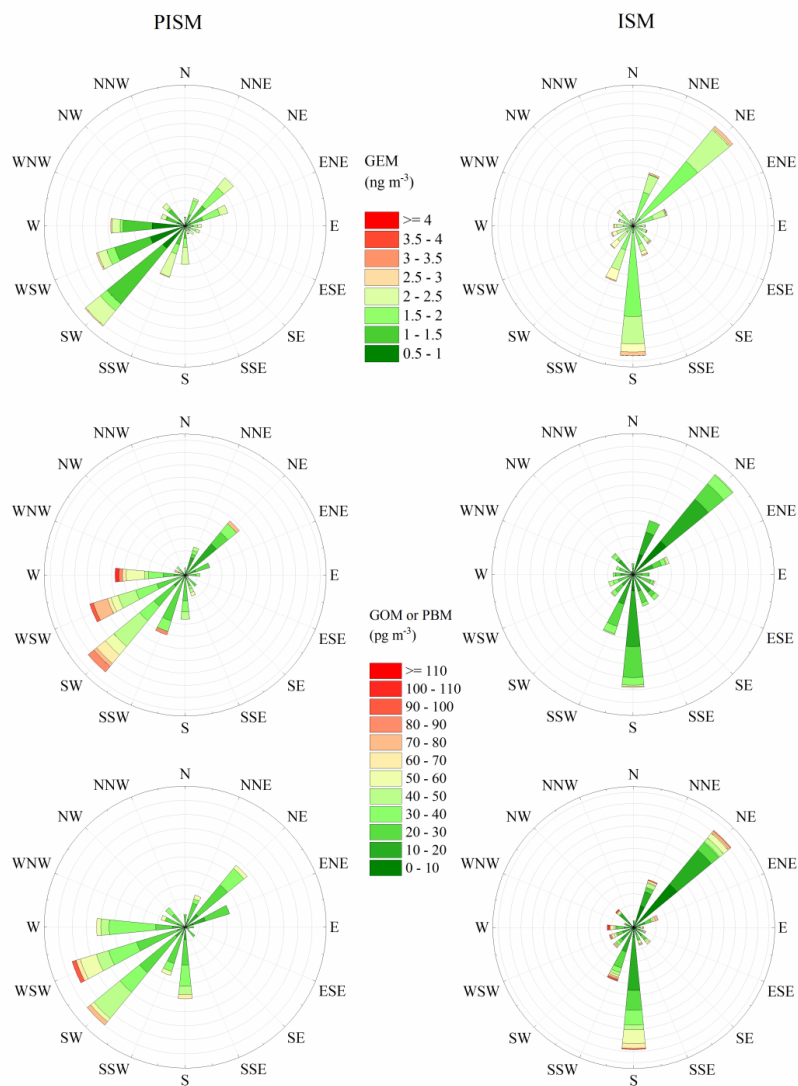


803

804



805
806 **Figure 4**



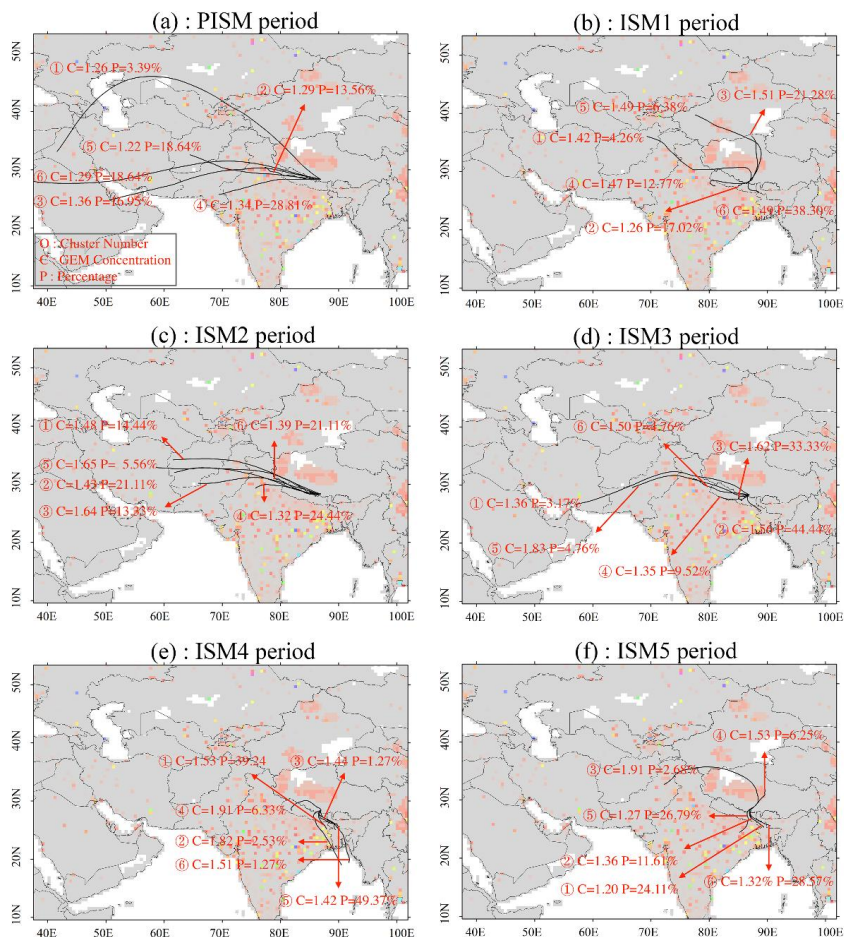
807
808



809

810 **Figure 5**

811

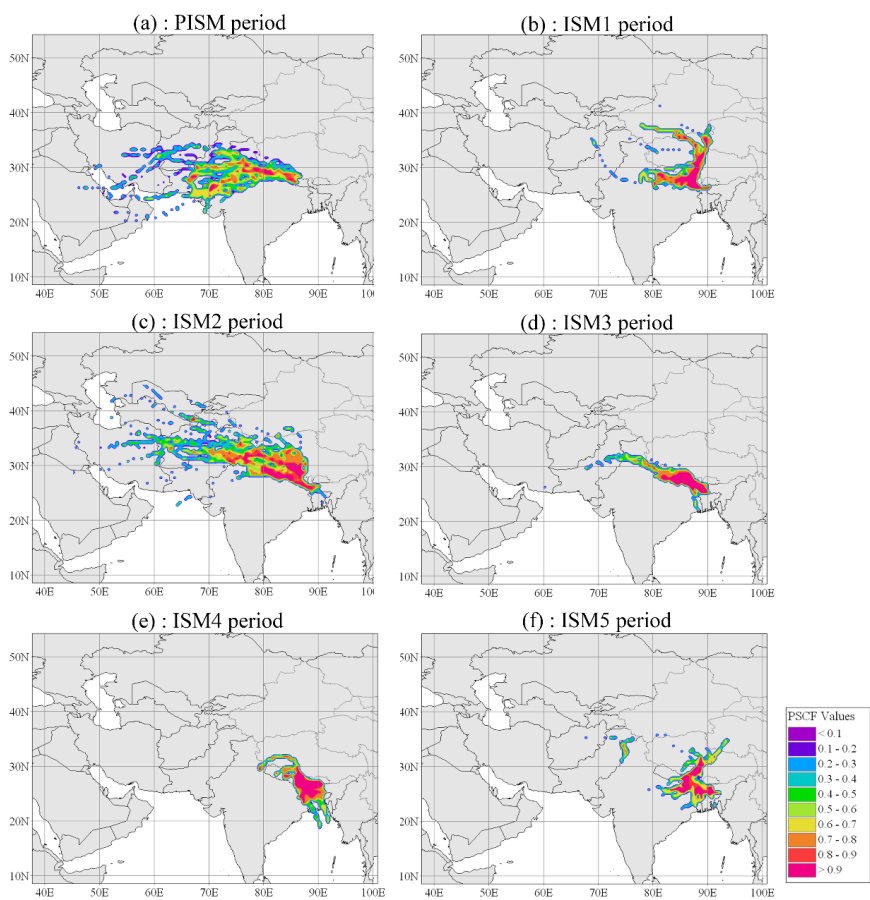


812

813



814 **Figure 6**



815

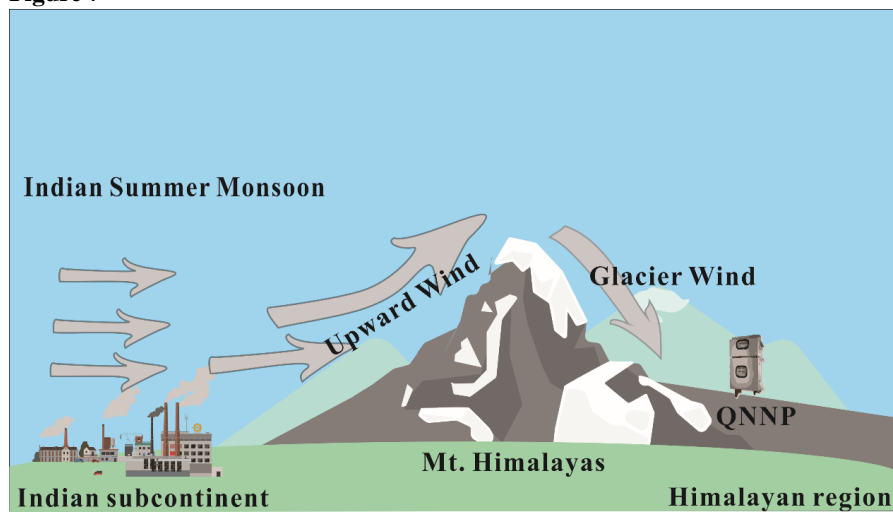
816

817

818



819 **Figure 7**



820
821



822

823 **Table 1. The statistics of GEM, GOM, PBM and meteorological variables in different**

824

episodes at QNNP

Period	Statistical	T (C°)	RH(%)	WS(m s ⁻¹)	GEM (ng m ⁻³)	GOM (pg m ⁻³)	PBM (pg m ⁻³)
PISM	Minimum	-5.6	1	0	0.54	11.6	9.4
	1st Qu.	1.6	11	1.8	0.99	21.7	22.3
	Median	6.4	25	3.6	1.19	29.5	26.9
	Mean	6.1	33	4.1	1.31	35.2	30.5
	3rd Qu.	11.2	53	6.3	1.58	42.8	36.1
	Maximum	16.3	89	13.9	2.91	101.3	92.6
ISM1	Min	-3.8	9	0	0.15	7.1	9.1
	1st Qu.	1.6	33	1.3	1.20	15.0	17.0
	Median	5.6	49	2.2	1.38	19.2	19.1
	Mean	5.6	50	2.7	1.44	20.2	21.2
	3rd Qu.	9.8	65	3.6	1.63	24.1	24.5
	Max	15.7	91	10.3	2.74	64.0	59.1
ISM2	Min	-1.3	3	0	0.47	3.9	12.4
	1st Qu.	4.1	30	1.3	1.14	18.5	40.4
	Median	8.5	48	2.2	1.35	23.7	54.8
	Mean	8.8	46	3.0	1.45	25.4	53.4
	3rd Qu.	13.7	64	4	1.68	31.3	64.9
	Max	19.6	87	11.2	3.74	63.4	106.3
ISM3	Min	2.6	26	0	0.78	3.2	0.8
	1st Qu.	8.1	44	1.3	1.33	14.5	12.4
	Median	11.8	58	2.7	1.51	18.9	17.1
	Mean	12.0	58	2.9	1.56	19.2	16.8
	3rd Qu.	15.6	73	4	1.72	23.4	22.0
	Max	21.8	92	9.9	2.70	36.6	31.3
ISM4	Min	6.0	25	0	0.66	6.7	0.3
	1st Qu.	9.3	43	1.3	1.35	12.9	10.6
	Median	12.1	61	2.7	1.46	18.0	17.3
	Mean	13.0	58	2.9	1.51	21.0	20.0
	3rd Qu.	16.6	72	3.6	1.61	24.9	26.1
	Max	22.7	90	9.9	2.62	149.1	78.6
ISM5	Min	2.2	18	0	0.48	0.8	0.2
	1st Qu.	8.3	59	0.9	1.17	7.2	6.2
	Median	10.7	75	2.2	1.35	10.7	9.4
	Mean	11.4	72	2.3	1.32	12.3	10.7
	3rd Qu.	14.1	86	3.1	1.49	16.0	14.1
	Max	22.9	96	9.4	2.45	121.3	33.2

825

826



Table 2. Summary of atmospheric Hg concentration and diurnal variation in previous studies and this study

Location	Elevation	Classification	Time period	GEM/(TGM)		GOM (pg m ⁻³)	PBM (pg m ⁻³)	GEM diurnal variation (Local time/GEM Conc.)			reference
				(ng m ⁻³)	(pg m ⁻³)			peak	valley	variation value	
Yorkville, Atlanta, USA	395	rural	2007-2008	1.35±0.17	8.55±18.8	4.43±5.59	-	11/1.37	6/1.32	0.05	(Nair et al., 2012)
Birmingham, Alabama, USA	-	urban	2005-2008	2.12±1.57	78.2±441.9	39.5±147.9	-	9/2.27	16/1.87	0.40	(Nair et al., 2012)
Pensacola, Florida, USA	-	rural	2005-2008	1.35±0.18	4.24±6.90	2.49±2.87	-	10/1.38	5/1.29	0.09	(Nair et al., 2012)
Mt. Waliguan, China	3816	remote	Sep 2007-Sep 2008	(1.98±0.98)	7.4±4.8	19.4±18.1	-	6/2.3	14/1.94	0.36	(Fu et al., 2012a)
Mt. Leigong, China	2178	remote	May 2008-May 2009	2.80±1.51	-	-	-	14/2.99	5/2.52	0.47	(Fu et al., 2010)
Mt. Gongga, China	1640	remote	May 2005-July 2006	(3.98)	-	-	-	11/4.45	2/3.55	0.90	(Fu et al., 2008)
Kodaikanal, India	2343	rural	Nov 2012-Sep 2013	(1.53±0.21)	-	-	-	16/1.66	7/1.43	0.23	(Karthik et al., 2017)
EvK2CNR, Nepal	5050	remote	Nov 2011-Apr 2012	(1.2±0.2)	-	-	-	18/1.3	6/1.1	0.1	(Gratz et al., 2013)
Shangri-La, China	3580	remote	Nov 2009-Nov 2010	(2.51±0.73)	8.22±7.9	38.32±31.26	-	17/2.48	6/1.71	0.77	(Zhang et al., 2015)
Colorado	3220	remote	April 2008-July 2008	1.6±0.3	20±21	9±6	-	20/3.40	10/3.00	0.40	(Fa ñ et al., 2009)
Miyun, China	220	rural	Dec 2008-Nov 2009	3.22±1.74	10.1±18.8	98.2±112.7	-	11/3.48	1/2.87	0.61	(Zhang et al., 2013)
Penghu Islands, China	25	coastal	Mar 2011-Jan 2012	(3.17±1.17)	-	-	-	8/1.00	17/0.92	0.08	(Jen et al., 2014)
Nome, China	5300	remote	Nov 2014-Mar 2015	0.95±0.19	-	-	-	-	-	-	(de Foy et al., 2016)
ALS, China	2450	remote	May 2011-May 2012	(2.09±0.63)	2.3±2.3	31.3±28.4	-	6/2.04	13/1.11	0.93	(Feng and Fu, 2016)
QNNP, China (this study)	4267	remote	Apr 2016-Aug 2016	1.42±0.37	21.3±13.5	25.5±19.2	-	-	-	-	This study